Energy &
Environmental Science

Cite this: *Energy Environ. Sci.*, 2012, **5**, 7601

www.rsc.org/ees

PAPER

Published on 20 April 2012. Downloaded by National Chiao Tung University on 28/04/2014 19:35:37.

Broadband and wide angle antireflection of sub-20 nm GaAs nanograss†

Srikanth Ravipati,[a] Jiann Shieh,*[b] Fu-Hsiang Ko,*[a] Chen-Chieh Yu,[c] Hsuen-Li Chen,[c] Chia-Tien Wu[a] and Szu-Hung Chen[d]

Received 6th March 2012, Accepted 20th April 2012
DOI: 10.1039/c2ee21558f

GaAs nanograss with diameters of less than 20 nm has been fabricated using a simple, one-step, maskless plasma etching-based approach. GaAs nanograss exhibits remarkable broadband antireflection properties, which arise from the graded refractive index between air and the GaAs substrate by the nanograss layer. Moreover, GaAs nanograss shows less sensitivity to transverse electric polarized light and transverse magnetic polarized light over a wide range of incident angles compared to the strong variation in a bare GaAs substrate. These effects show that sub-20 nm GaAs nanograss with lengths of approximately 200 nm has an enhanced absorption of 98–100% when the incident energy is larger than the GaAs bandgap (λ = 240–873 nm) and an enhanced absorption of 72–98% when the incident energy is less than the bandgap (λ = 873–2400 nm). Our simple, one-step, and maskless plasma etching method opens a promising approach for the direct implementation of broad omnidirectional antireflective surfaces on solar cells and various optoelectronic devices to improve device performance.

Introduction

Nanostructure-based broadband antireflection coatings[1–3] inspired by moths' eyes[4,5] have attracted attention because of their fascinating optical properties unobserved in conventional multilayer antireflection coatings. Such antireflection behavior arises from the graded index profile between air and the substrate. Compared with conventional multilayer coatings, the polarization-insensitive, broadband, and omnidirectional aspects of the graded-index nanostructure-based antireflection coating make it an ideal candidate for efficient solar cells. In this study, we present a one-step and maskless plasma etching fabrication method for omnidirectional nanostructures of gallium arsenide (GaAs). The process is simple, low-cost, high-throughput, and can create large-area sub-20 nm nanostructures over an entire wafer.

Compared with Si-based devices, GaAs-based photonic devices have attracted considerable interest because of their direct bandgaps and high absorption coefficients.[6–10] Further improved light absorption efficiency can be achieved by broadband antireflection coatings for these devices. For example, self-assembled microspheres,[11] ITO nanocolumns,[12] plasmonic nanoparticles,[13] and nanoimprinting structures[14] have been used as antireflection coatings for solar cells; graded-index ITO,[15] subwavelength gratings,[16] and pillars[17] have been used for LEDs. However, it has been difficult to implement broadband antireflection coatings made with the same materials as the devices rather than using

[a]*Institute of Nanotechnology, Department of Materials Science & Engineering, National Chiao Tung University, Hsinchu 30010, Taiwan (ROC). E-mail: fhko@mail.nctu.edu.tw; Fax: +886-35744689; Tel: +886-35712121 ext. 55803*
[b]*Department of Materials Science & Engineering, National United University, Miaoli 36003, Taiwan (ROC). E-mail: jshieh@nuu.edu.tw; Fax: +886-37382247; Tel: +886-37382244*
[c]*Department of Materials Science and Engineering, National Taiwan University, Taipei 10617, Taiwan (ROC)*
[d]*National Nano Device Laboratories, Hsinchu 30078, Taiwan (ROC)*
† Electronic supplementary information (ESI) available. See DOI: 10.1039/c2ee21558f

Broader context

GaAs is an important material for photovoltaic devices because of its superior direct bandgap and high absorption coefficient. Its large refractive index, however, raises the reflectance of incident light in the range of UV to NIR. Subwavelength nanostructures on the surface can reduce the reflectance and enhance absorption. However, creating nanostructures much smaller than the incident wavelength is expensive and time consuming. Here we demonstrate an efficient method to fabricate sub-20 nm GaAs nanostructures with high uniformity over a whole wafer using a hydrogen plasma process. For a structure featuring a thickness of 200 nm, the wide-angle reflectance can be reduced by more than one order over broadband wavelengths of incident light. GaAs-based optoelectronics can be improved with this nanograss surface in the future.

Published on 20 April 2012. Downloaded by National Chiao Tung University on 28/04/2014 19:35:37.

a foreign material such as ITO, Ag, or SiO_2. Nevertheless, subwavelength gratings (SWGs) and subwavelength structures (SWSs) of GaAs,[16–27] inspired from moth-eye principles, can suppress the Fresnel reflection by gradually and continuously changing the refractive index at the interface of air and a substrate material, and have antireflection properties in the broadband wavelength range. To obtain SWGs and SWSs with a broadband antireflection nature, many fabrication methods have been proposed, including electron-beam lithography,[18–20] interference lithography,[21,22] holographic lithography,[23] colloidal or nanosphere lithography,[24–27] and thermally dewetted metallic nanoparticles as etch masks followed by dry etching.[28] However, these methods may require multiple steps and may be expensive and time-consuming. Developing new fabrication approaches, especially lithography-free, maskless, low-cost, and one-step fabrication methods for omnidirectional antireflective surfaces, is one of the key issues in renewable and nonpolluting energy production. Recently, researchers have developed a new one-step, inexpensive approach to the maskless fabrication of silicon nanograss through hydrogen plasma etching in the absence of a catalyst.[29–33] Plasma nanofabrication has successfully fabricated well-aligned single crystalline silicon nanograss without requiring masking materials. The basic concept behind the hydrogen plasma etching process is using plasma as an efficient means of producing active hydrogen atoms to react with the materials placed in the hydrogen plasma to form volatile hydride compounds. Antireflection properties of silicon nanograss etched for 40 min below 4.5% have been obtained between DUV and near-IR (200–900 nm).[32]

The present study used a hydrogen plasma-based approach to create nanograss on GaAs surfaces. We expected that GaAs could be etched using hydrogen because the Ga–H bond strength is 276 kJ mol^{-1} and the As–H bond strength is 319 kJ mol^{-1}, both of which are stronger than the Ga–As bonds in bulk GaAs (202 kJ mol^{-1}), and because the reaction products are volatile at low temperatures.[34] The density and height of these nanostructures can be controlled by etching time alone. Moreover, the antireflection performance of GaAs nanostructures is almost independent of the polarization of the incident light over a wide range of angles of incidence (AOI), showing excellent omnidirectional antireflection performance. These optical properties suggest a promising approach to enhance optical absorption efficiency of solar cells over an entire wafer.

Experiment

The GaAs nanograss was prepared by hydrogen plasma etching in an inductively coupled plasma chemical vapor deposition (ICPCVD) system. The chamber was cleaned with CF_4 and O_2 plasma before performing the etching process; it was evacuated to a base pressure of 5×10^{-5} Torr with a substrate holder heated at 300 °C. After cleaning the chamber, a 2-in. single-side polished N-type GaAs (100) wafer (AXT, Inc., US) without precleaning was loaded into the chamber. After loading the GaAs wafer, H_2 gas (165 sccm) was introduced and then the reactor pressure (30 mTorr) was maintained. We used a 13.56 MHz inductively coupled plasma (ICP) to dissociate hydrogen gas and obtain a high density of hydrogen radicals, and then bombarded the substrate with these species. The radio frequency (RF) power was 550 W and the bias power was 280 W. The sample materials were analyzed using a scanning electron microscope (SEM, JEOL JSM-6500F) and a transmission electron microscope (TEM, JEOL JEM-2010F) equipped with an energy-dispersive X-ray (EDX) analyzer. Wavelength-dependent transmission and reflection measurements for wavelengths between 5.16 eV (λ = 240 nm) and 0.516 eV (λ = 2400 nm) were achieved by mounting the sample and detector on a set of computer-controlled rotation stages. The samples were illuminated using the collimated beam of a fiber-coupled halogen lamp (Yokogawa AQ4303), and the optical spectra were obtained using a Hitachi U-4100 various-angle optical UV-Vis-NIR spectrometer.

Results and discussion

SEM images in Fig. 1(a)–(e) show that GaAs nanograss was successfully fabricated using hydrogen plasma etching. Similar to Si nanograss,[29,32] the GaAs nanograss is characterized by high uniformity and nanoscale size. The diameter of the nanograss was 20 nm, which is substantially smaller than that obtained by dewetting-mask-assisted[28] or colloid-mask-assisted etching.[24] In Fig. 1(f) we illustrate the associated change in the measured height and density with respect to the etching time. Initially, as the etching time increased, the height and aspect ratios of GaAs nanostructures increased vertically, whereas the density of nanostructures decreased because the neighboring nanograss clumped with each other. However, with a further increase of etching time (longer than 180 min), the nanograss shortened, and the density increased again, implying that for clumped nanograss the hydrogen ions broke the bundles instead of etching them further. The length of nanograss has a maximum of 200 nm at an etching time of 180 min, and all the nanograss is characterized by an ultrahigh surface density ($>10^{11}$ cm^{-2}).

The cross-sectional SEM image in Fig. 2a shows that the average height of GaAs nanostructures etched for 120 min is

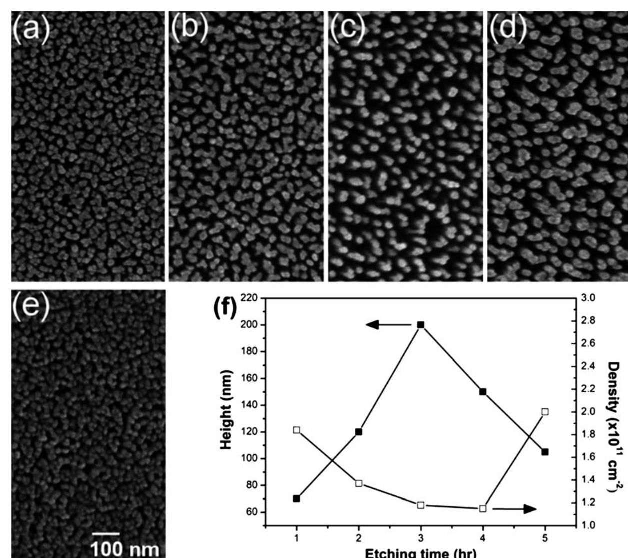

Fig. 1 (a–e) Plane-view SEM images of GaAs nanograss etched for 60, 120, 180, 240 and 300 min; (f) average heights and densities of the GaAs nanograss etched for 60, 120, 180, 240 and 300 min were 70, 120, 200, 150 and 105 nm and 1.84×10^{11}, 1.37×10^{11}, 1.18×10^{11}, 1.15×10^{11} and 2.0×10^{11} per cm^2, respectively.

This journal is © The Royal Society of Chemistry 2012

View Article Online

Published on 20 April 2012. Downloaded by National Chiao Tung University on 28/04/2014 19:35:37.

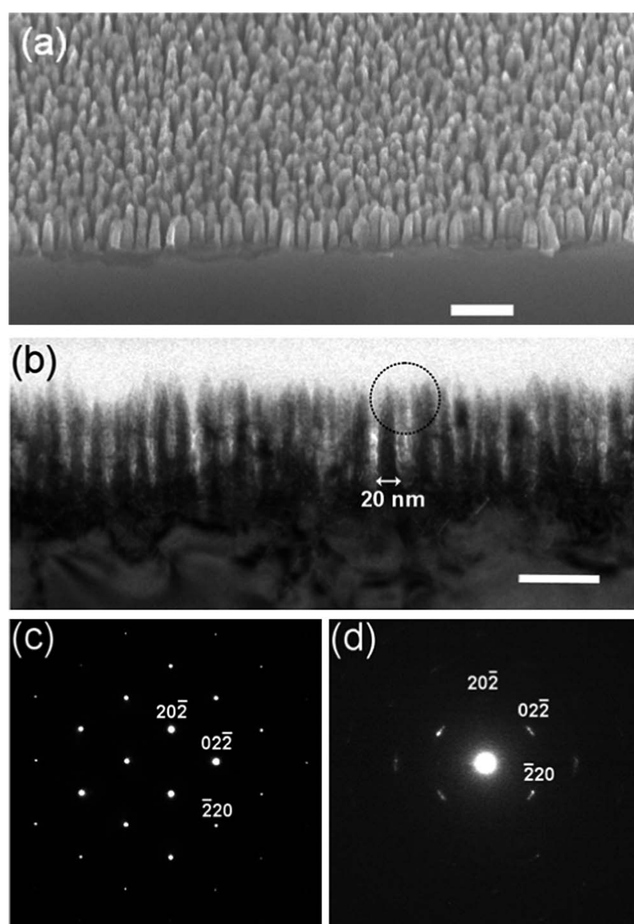

Fig. 2 (a) Cross-sectional SEM images of GaAs nanograss etched for 120 min. Scale bars represent 200 nm; (b) cross-sectional TEM images of GaAs nanograss etched for 120 min. Scale bars represent 100 nm; (c) a SAD pattern recorded from the bottom of the nanograss; (d) a SAD pattern recorded from the circled region in (b).

approximately 120 nm. The tip diameter was only approximately 10 nm and the base diameter was approximately 20 nm. Vertically aligned GaAs nanostructures are evident from a typical cross-sectional bright-field TEM image of the sample etched for 120 min as shown in Fig. 2b. Each nanostructure had a solid core of single-crystalline GaAs covered with a thin amorphous layer on both the sidewall and tip of the nanostructures because of plasma bombardment on the nanostructures. The selective area diffraction (SAD) pattern shown in Fig. 2c from the region near the base had a zinc-blend single-crystal structure. The diffusive ring pattern (Fig. 2d), selected from the circled region in Fig. 2c originated from the bended nanograss and indicates that the nanograss was clumped together. EDX analysis (ESI, Fig. S1†) shows that some metal impurities were present at the top of the GaAs nanostructures in addition to GaAs, which may originate from contamination sputtered from the chamber. The presence of metal impurities gradually disappears from the top to the bottom regions of the nanostructures, and high Ga and As peaks are observed at the bottom of nanostructures.

We determined the broadband specular reflection and direct transmission for the samples over the UV-Vis-NIR regions (240–2400 nm), together with a bulk GaAs wafer for reference (Fig. 3). The reflection was measured at an incident angle of 5° with respect to the normal of surface, whereas the transmission was measured at normal incidence. Fig. 3a shows the reflectance as a function of wavelength for various etching process times

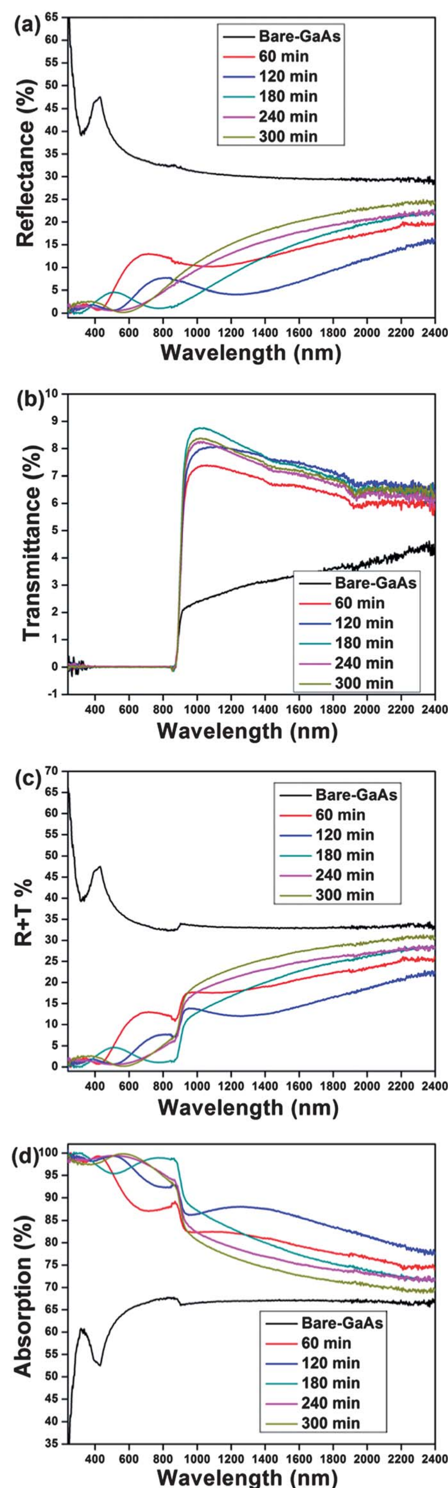

Fig. 3 (a) The measured reflectance at a 5° AOI, (b) the measured transmittance for normal incidence, (c) the sum of measured reflectance and transmittance, and (d) the absorption ($1 - T - R$) as a function of wavelength for different heights and densities of GaAs nanograss. The measurements of bare GaAs are shown for comparison.

View Article Online

Published on 20 April 2012. Downloaded by National Chiao Tung University on 28/04/2014 19:35:37.

ranging from 60 to 300 min. The reflectance of the polished GaAs substrate was 31–49% from $\lambda = 240–2400$ nm, and the reflectance for GaAs nanograss was significantly reduced compared to bulk GaAs. After a 120 min etching, the wavelength-averaged reflectance of nanograss was one order smaller than that of the bulk wafer (38.65% between 240 and 873 nm). The lowest reflectance was less than 1% at some specific wavelength. The broad maximum presented in the reflection spectra indicates that the GaAs nanograss also behaved as a thin film with a lower effective refractive index. When incident light was reflected from the air/nanograss and nanograss/substrate interfaces, they could interfere with each other to make these oscillations.

The measured transmittances as a function of wavelength for the fabricated nanostructures on GaAs substrate are displayed in Fig. 3b. The transmittance of a polished GaAs substrate is also shown as a reference from 240 to 2400 nm. The sharp edge visible for all samples at 1.42 eV (λ = 873 nm) is due to bandgap absorption.[28,35,36] For low energies, the transmittance of the GaAs substrate increases from 2% at 1.42 eV ($\lambda = 873$ nm) to 4% at 0.516 eV (λ = 2400 nm). The transmittance of all nanostructured samples is higher than that of bare GaAs. The enhanced transmittance shown in Fig. 3b and the reduced reflectance of these GaAs nanostructures are due to the graded refractive index, which provides impedance matching between air and GaAs. For GaAs nanograss, the sum of reflectance and transmittance measurements was reduced with respect to the bare GaAs substrate (>32.6% when above bandgap) (Fig. 3c), which indicates that the enhanced absorption was facilitated by the nanograss structure.

Fig. 3d shows the optical absorption of GaAs nanograss and bare GaAs samples. The absorption is calculated by the expression $A = 1 - R - T$, where T is the transmittance and R is the reflectance. All the nanostructured samples show high absorption compared with bare GaAs, depending on the length and density of the nanostructures. The absorption by the GaAs substrate is limited to <67% from $\lambda = 240$ to 2400 nm, due to the large reflectance shown in Fig. 3a. For incident energies larger than the bandgap of GaAs, nanograss shows a high absorption, which is substantially larger than that of bare GaAs in the UV-Vis range (35–67%). When the incident energy was lower than the bandgap (873–2400 nm), GaAs nanograss still kept a high absorption. The highest absorption value observed was 98–100% (above the bandgap of GaAs) and 72–98% (below the bandgap of GaAs) for the 200 nm-thick nanograss sample.

For effective broadband and omnidirectional antireflection, the antireflective structure must exhibit low reflectance over a wide range of AOI for polarized light.[12] This is beneficial for photovoltaics without an incorporated tracking system because broadband omnidirectionality is the central problem of collection efficiency under full-day solar radiation.[37] At normal incidence the reflection is irrelevant to the polarization. However, the reflection strongly depends on the polarization when the AOI is non-zero. To investigate broadband and omnidirectional characteristics, we performed specular reflection measurements of GaAs nanostructures as a function of wavelength from 350 to 1200 nm and for AOI from 20 to 60° for samples etched for 120 min with transverse electric (TE) and transverse magnetic (TM) polarized lights. TE denotes planes of incidence perpendicular to the electric field, whereas TM denotes planes of incidence parallel to the electric field. The results are shown in Fig. 4a and b. Fig. 5a shows that both TE reflectance of bare GaAs wafer and GaAs nanograss increased with AOI, but the angular reflectance of GaAs nanograss was much lower than that of bare GaAs substrate, confirming the excellent wide-angle antireflection characteristics. The TM reflectance of bare GaAs, shown in Fig. 5b, reduced with the AOI and approached its Brewster angle. But for the GaAs nanograss sample, reduced TM reflectance with less sensitivity respective to the AOI was found and it quickly reached the Brewster angle, which may occur from incoherent multiple scattering.[38]

Conclusion

We developed a one-step and maskless plasma process to create omnidirectional broadband antireflective GaAs nanograss with ultra-high uniformity over a whole wafer. We find that the surface reflection can be reduced by one order over broadband wavelength and both transmission and absorption were

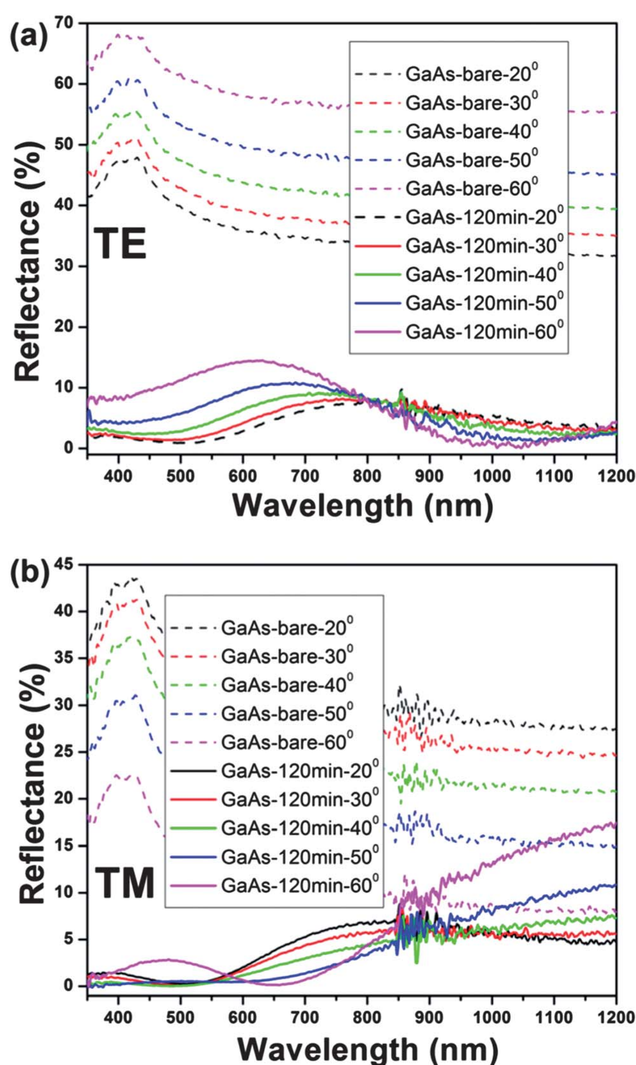

Fig. 4 The specular reflectance as a function AOI for (a) TE for 120 min and (b) TM for 120 min etched samples over a range from 350 to 1200 nm. The TE and TM polarized light reflectance of the bare GaAs substrate are also presented in figures for comparison.

 This journal is © The Royal Society of Chemistry 2012

View Article Online

Published on 20 April 2012. Downloaded by National Chiao Tung University on 28/04/2014 19:35:37.

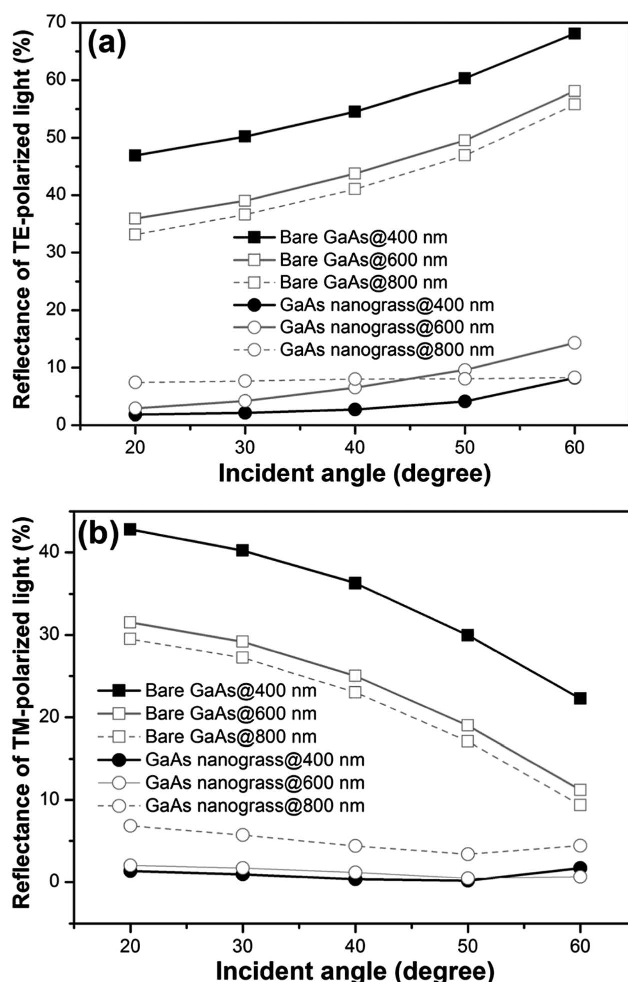

Fig. 5 The angle-dependent reflectance of AOI covering 20 to 60° for 400, 600 and 800 nm (a) TE and (b) TM for polarization for samples etched for 120 min. The TE and TM polarization of the bare GaAs substrate is also presented for comparison.

enhanced in these GaAs nanograss layers. The diameter of each nanograss blade was less than 20 nm, and the thickness of the nanograss layer was less than 200 nm. These antireflection nanostructures also exhibit low reflectance over a wide range of AOI for TE and TM polarized light. The remarkable antireflection properties over a broad wavelength and wide angular range demonstrate that this simple wafer-scale fabrication method provides promising potential for solar cells and various optoelectronic devices to improve their performance.

Acknowledgements

The authors acknowledge financial support from National Science Council under grants NSC100-2221-E239-012-MY2.

References

1 Y. F. Huang, S. Chattopadhyay, Y. J. Jen, C. Y. Peng, T. A. Liu, Y. K. Hsu, C. L. Pan, H. C. LO, C. H. Hsu, Y. H. Chang, C. S. Lee, K. H. Chen and L. C. Chen, *Nat. Nanotechnol.*, 2007, **2**, 770.
2 J. Q. Xi, M. F. Schubert, J. K. Kim, E. F. Schubert, M. Chen, S. Y. Lin, W. Liu and J. A. Smart, *Nat. Photonics*, 2007, **1**, 176.
3 S. L. Diedenhofen, G. Vecchi, R. E. Algra, A. Hartsuiker, O. L. Muskens, G. Immink, E. P. A. M. Bakkers, W. L. Vos and J. G. Rivas, *Adv. Mater.*, 2009, **21**, 973.
4 P. B. Clapham and M. C. Hutley, *Nature*, 1973, **244**, 281.
5 D. G. Stavenga, S. Foletti, G. Palasantzas and K. Arikawa, *Proc. R. Soc. London, Ser. B*, 2006, **273**, 661.
6 T. Yamada, A. Moto, Y. Iguchi, M. Takahashi, S. Tanaka, T. Tanabe and S. Takagishi, *Jpn. J. Appl. Phys.*, 2005, **44**, L985.
7 R. R. King, D. C. Law, K. M. Edmondson, C. M. Fetzer, G. S. Kinsey, H. Yoon, R. A. Sherif and N. H. Karam, *Appl. Phys. Lett.*, 2007, **90**, 183516.
8 C. Algora, E. Ortiz, I. Rey-Stolle, V. Diaz, R. Peia, V. Andreev, V. Khvostikov and V. Rumyantsev, *IEEE Trans. Electron Devices*, 2001, **48**, 840.
9 R. R. LaPierre, *J. Appl. Phys.*, 2001, **110**, 014310.
10 E. Oliva, F. Dimroth and A. W. Bett, *Progr. Photovolt.: Res. Appl.*, 2008, **16**, 289.
11 T. H. Chang, P. H. Wu, S. H. Chen, C. H. Chan, C. C. Lee, C. C. Chen and Y. K. Su, *Opt. Express*, 2009, **17**, 6519.
12 P. Yu, C. H. Chang, C. H. Chiu, C. S. Yang, J. C. Yu, H. C. Kuo, S. H. Hsu and Y. C. Chang, *Adv. Mater.*, 2009, **21**, 1618.
13 K. Nakayama, K. Tanabe and H. A. Atwater, *Appl. Phys. Lett.*, 2008, **93**, 121904.
14 K. S. Han, J. H. Shin, W. Y. Yoon and H. Lee, *Sol. Energy Mater. Sol. Cells*, 2011, **95**, 288.
15 J. K. Kim, S. Chhajed, M. F. Schubert, E. F. Schubert, A. J. Fischer, M. H. Crawford, J. Cho, H. Kim and C. Sone, *Adv. Mater.*, 2008, **20**, 801.
16 Y. Kanamori, M. Ishimori and K. Hane, *IEEE Photonics Technol. Lett.*, 2002, **14**, 1064.
17 Y. M. Song, E. S. Choi, J. S. Yu and Y. T. Lee, *Opt. Express*, 2009, **17**, 20991.
18 J. R. Wendt, G. A. Vawter, R. E. Smith and M. E. Warren, *J. Vac. Sci. Technol., B*, 1996, **14**, 4096.
19 R. E. Smith, M. E. Warren, J. R. Wendt and G. A. Vawter, *Opt. Lett.*, 1996, **21**, 1201.
20 K. Wensun, S. C. Huang, A. Kechiantz and C. P. Lee, *Opt. Quantum Electron.*, 2005, **37**, 425.
21 Y. M. Song, S. J. Jang, J. S. Yu and Y. T. Lee, *Small*, 2010, **6**, 984.
22 Y. M. Song, S. Y. Bae, J. S. Yu and Y. T. Lee, *Opt. Lett.*, 2009, **34**, 1702.
23 X. Chen, Z. C. Fan, J. Zhang, G. F. Song and L. H. Chen, *Chin. Phys. Lett.*, 2010, **27**, 124210.
24 C. H. Sun, B. J. Ho, B. Jiang and P. Jiang, *Opt. Lett.*, 2008, **33**, 2224.
25 D. S. Kim, M. S. Park and J. H. Jang, *J. Vac. Sci. Technol., B: Microelectron. Nanometer Struct.–Process., Meas., Phenom.*, 2011, **29**, 020602.
26 B. J. Kim and J. Kim, *Opt. Express*, 2011, **19**, A326.
27 B. J. Kim, J. Bang, S. Jang, D. Kim and J. Kim, *Thin Solid Films*, 2010, **518**, 6583.
28 J. W. Leem, J. S. Yu, Y. M. Song and Y. T. Lee, *Sol. Energy Mater. Sol. Cells*, 2011, **95**, 669.
29 M. C. Yang, J. Shieh, C. C. Hsu and T. C. Cheng, *Electrochem. Solid-State Lett.*, 2005, **8**, C131.
30 J. Shieh, F. J. Hou, Y. C. Chen, H. M. Chen, S. P. Yang, C. C. Cheng and H. L. Chen, *Adv. Mater.*, 2010, **22**, 597.
31 S. Ravipati, C. J. Kuo, J. Shieh, C. T. Chou and F. H. Ko, *Microelectron. Reliab.*, 2010, **50**, 1973.
32 J. Shieh, C. H. Lin and M. C. Yang, *J. Phys. D: Appl. Phys.*, 2007, **40**, 2242.
33 J. Shieh, S. Ravipati, F. H. Ko and K. Ostrikov, *J. Phys. D: Appl. Phys.*, 2011, **44**, 174010.
34 Y. R. Luo, in *Comprehensive Handbook of Chemical Bond Energy*, CRC press, 2007.
35 S. Kasap, C. Koughia, J. Singh, H. Ruda and S. K. O'Leary, in *Springer Handbook of Electronic and Photonic Materials*, ed. S. Kasap and P. Capper, Springer, 2006, ch. 3, pp. 47–77
36 M. L. Kuo, D. J. Poxson, Y. S. Kim, F. W. Mont, J. K. Kim, E. F. Schubert and S. Y. Lin, *Opt. Lett.*, 2008, **33**, 2527.
37 H. A. Macleod, *Thin Film Optical Filters*, Taylor & Francis, London, UK, 3rd edn, 2001.
38 Y. C. Chao, C. Y. Chen, C. A. Lin and J. H. He, *Energy Environ. Sci.*, 2011, **4**, 3436.